I&EC research
Industrial & Engineering Chemistry Research

pubs.acs.org/IECR

Article

CVD-Deposited Oxygen-Selective Fluorinated Siloxane Copolymers as Gas Diffusion Layers

Gizem Cihanoğlu and Özgenç Ebil*

Cite This: *Ind. Eng. Chem. Res.* 2022, 61, 2633−2642

Read Online

ACCESS | Metrics & More | Article Recommendations | Supporting Information

Downloaded via IZMIR YUKSEK TEKNOLOJI ENSTITUSU on March 9, 2022 at 08:30:15 (UTC).
See https://pubs.acs.org/sharingguidelines for options on how to legitimately share published articles.

ABSTRACT: Copolymer thin films of 2,4,6,8-tetramethyl-2,4,6,8-tetravinylcyclotetrasiloxane (V4D4), 2-(perfluorohexylethylacrylate) (PFHEA), and 2-(perfluoroalkylethylmethacrylate) (PFEMA) were synthesized via initiated chemical vapor deposition (iCVD) as potential candidates for gas diffusion layers (GDLs) in gas diffusion electrodes (GDEs) for aqueous metal−air batteries. Thin-film GDLs exhibited an average water vapor transmission rate of 7.5 g m^{-2} day^{-1} and enhanced oxygen diffusion with oxygen permeabilities as high as 3.53 × 10^{-15} mol m m^{-2} s^{-1} Pa^{-1} (10.5 Barrer). The electrochemical performance of GDEs fabricated using commercial catalysts, current collectors, and synthesized GDLs was investigated by cyclic voltammetry, electrochemical impedance spectroscopy, and potentiodynamic polarization measurements. The fabricated GDEs exhibited higher oxygen reduction current densities (228.2 mA cm^{-2}) compared to commercial GDEs (132.7 mA cm^{-2}). Copolymer GLDs exhibited an order of magnitude higher oxygen diffusion (39.5 × 10^{-8} cm^2 s^{-1}) in GDEs compared to commercial counterparts (1.84 × 10^{-8} cm^2 s^{-1}). Due to the high oxygen solubility of V4D4 and excellent hydrophobic behavior of PFHEA and PFEMA, their copolymers can effectively promote the diffusion of oxygen and restrict moisture intake, making them ideal materials for GDLs. Combining well-balanced properties of siloxane and fluorinated polymer chemistries, the iCVD process is an excellent low-cost method for the fabrication of GDLs for metal−air battery applications.

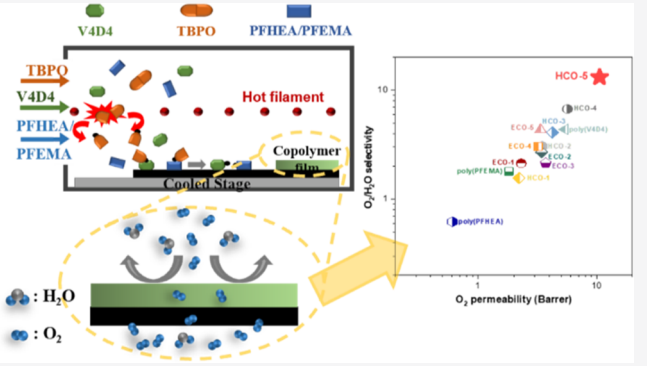

1. INTRODUCTION

As the worldwide demand for energy storage grows rapidly, electrochemical energy storage technologies, mainly batteries have attracted a lot of attention. The primary requirement for energy storage systems, ranging from small portable electronic devices to large electric vehicles, is stable electrochemical performance with high energy and power density, long cycle life, and high depth of discharge.[1−3] Rechargeable batteries including Pb-acid, Ni−Cd, NiMH, and Li-ion are the most commonly used battery technologies for stationary energy storage applications. Due to higher energy and power densities, Li-ion batteries are in a better position to compete with other battery technologies that are commercially available today. However, Li-ion batteries suffer from several issues including safety, availability and cost of raw materials used in manufacturing, and environmental impact. Therefore, new approaches and considerable efforts to develop efficient, scalable, sustainable, and environmentally friendly "beyond Li-ion" storage solutions are needed. In recent years, metal−air batteries have received much attention as the next-generation energy storage solution due to their higher theoretical energy density (1,000−13,000 W h kg^{-1}) and lower weight compared to current energy storage systems.[1] Today's metal−air batteries are mostly primary batteries, in which the capacity of the battery usually depends on the capacity of the metal electrode. However, electrochemical stability of the gas diffusion electrode (GDE) is also important for the overall performance of metal−air batteries. Metal air batteries did not reach their full potential due to problems associated with electrode reversibility and electrochemical stability. Even today's commonly used metal−air battery is a century old alkaline zinc−air battery (ZAB) found only limited use in medical and tele-communication applications. In addition to problems associated with specific metal electrodes, the development of metal−air batteries is largely hindered by critical challenges related to the reversibility and lifetime of GDEs, in which a gas reactant comes in contact with a liquid reaction medium. A typical GDE is made of a porous hydrophobic membrane (gas diffusion layer, GDL), a catalytic layer (active layer), and a current collector. Although most efforts are focused on the

Received: October 26, 2021
Revised: January 2, 2022
Accepted: January 10, 2022
Published: February 4, 2022

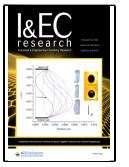

ACS Publications

© 2022 American Chemical Society

https://doi.org/10.1021/acs.iecr.1c04244
Ind. Eng. Chem. Res. 2022, 61, 2633−2642

synthesis of bifunctional catalysts and carbon-free catalytic layers, the role of GDLs on the GDE performance should not be overlooked.[4] Moisture penetration from the atmosphere is one of the major problems for alkaline metal−air batteries since it leads to the formation of insoluble products. The moisture also restricts oxygen diffusion through the electrode which can severely reduce the electrochemical activity of the cathode.[5,6] In addition, the water uptake through the cell leads to a decreased electrolyte concentration, considerably reducing ionic conductivity and deteriorating cycling life.[7,8] Therefore, most of the current studies in the literature related to metal−air batteries have reported cycling ability and rate ability in dry O_2 atmosphere.[9−14] Another problem associated with metal−air batteries is excessive water loss from the electrolyte, negatively affecting discharge reactions during long-term operation.[15−17] The thickness of the air electrode may also hinder mass transfer of oxygen as well as the capacity and rate of performance of the metal−air batteries.[18,19] Oxygen transport limitation and oxygen starvation during cathode reactions at high current densities results in serious charge/discharge polarization and poor rate performance.[20,21]

To enhance the oxygen permeability and reduce the permeation of moisture and electrolyte evaporation, different approaches with varying success have been studied such as impregnation of a proton conductor (such as Nafion) into the catalyst layer[22,23] and changing the chemical composition[21,24] and thickness[18] of GDLs. Zhang et al. fabricated Li−air batteries with an oxygen selective air electrode for operation in ambient air (20−30% RH) for more than a month.[21,25] Yue et al. employed proton-doped conductive polyaniline films for Li−air batteries to restrict the moisture intake and electrolyte evaporation through the cell.[20] Crowther at al. applied an O_2-selective membrane based on polysiloxane and methacrylate-polysiloxane copolymers for Li−air batteries to preclude water transport from the atmosphere.[8] In a similar study, Bodoardo et al. reported that the silicone oil-wetted poly(vinylidene fluoride-*co*-hexafluoropropylene) (PVDF-HFP) film as the oxygen-selective membrane was effective to retain moisture and prevent membrane dehydration.[5] A PVDF-HFP matrix consisting of dextrin-nanosponge to entrap moisture from air was also investigated.[6] Lu et al. applied oxygen-selective membranes based on polymers and metal−organic framework containing −OH and $-NH_2$ groups to effectively trap H_2O and CO_2.[24] Non-solvent-induced phase separation,[5,6,24] solution deposition,[16,21] and evaporation-deposition[26] are commonly used methods to fabricate GDLs with oxygen selectivity and water permeation resistance. However, both methods suffer from poor conformality and limited thickness control on the surface. Most GDLs in today's GDEs for metal−air batteries cannot separate O_2 and H_2O based on bulk or Knudsen diffusion due to higher diffusivity and smaller molecular diameter of H_2O.[15,24,27] An ideal GDL should have high oxygen permeability and serve as a moisture barrier. Two specific material groups seem to be promising candidates for the fabrication of the ideal GDL: (1) polymer membranes containing siloxane with extremely high oxygen solubility and thermal stability and (2) hydrophobic perfluorinated polymers with high chemical and thermal stability in addition to high oxygen solubility to suppress the moisture uptake and electrolyte evaporation. Although copolymers of these specific materials could meet the requirements for GDL, it is also necessary to employ a low-cost and scalable technique that can fabricate GDLs in various geometries and dimensions.

Here, we report the synthesis of thin copolymer films of 2,4,6,8-tetramethyl-2,4,6,8-tetravinylcyclotetrasiloxane (V4D4), 2-(perfluorohexylethylacrylate) (PFHEA), and 2-(perfluoroalkylethylmethacrylate) (PFEMA) via initiated chemical vapor deposition (iCVD) for potential candidates as GDL materials. Due to the high oxygen solubility of V4D4 and excellent hydrophobic behavior of PFHEA and PFEMA, their copolymers can effectively promote the diffusion of oxygen and restrict the moisture intake. Although we did not attempt to address any issues related to bifunctional catalyst layers and current collectors, we also report the electrochemical performance of GDEs fabricated using commercially available catalysts and current collectors as active layers and iCVD-deposited copolymer GDLs. To the best of our knowledge, this is the first study in the literature where poly(V4D4-*co*-PFHEA) and poly(V4D4-*co*-PFEMA) copolymer coatings are fabricated and implemented as GDLs in battery applications.

2. MATERIALS AND METHODS

2.1. Materials. Analytical grade chemicals, V4D4 (Sigma-Aldrich, 97%), 2-(perfluorohexylethyl)acrylate (PFHEA, Fluoryx Inc., >99%), and 2-(perfluoroalkyl)ethylmethacrylate (PFEMA, Fluoryx Inc., >93%) as monomers and *tert*-butyl peroxide (TBPO, Sigma-Aldrich, 98%) as the initiator, were used for the fabrication of copolymer thin films. Polysulfone (Psf) (Sigma-Aldrich, MW 26,000) and chloroform (Sigma-Aldrich) were used for the preparation of the support membrane used during water vapor permeability (WVP) measurements due to high water permeability of Psf.[28,29]

2.2. Preparation of Support Membranes. Psf was used as the supporting membrane/substrate for water vapor and oxygen permeability measurements. To fabricate the support membranes, Psf was heated at 140 °C for 3 h under vacuum to remove absorbed water. To obtain 12 wt % Psf solution, 2.05 g of Psf was dissolved in 10 mL of chloroform and stirred for 24 h to obtain a viscous solution. About 10 mL of Psf solution was dispensed on a glass substrate (2.5 cm × 2.5 cm), which was then spun at 1500 rpm for 30 s in a spin coater (Laurell, Model WS-650MZ-23NPPB0), followed by drying at 70 °C for 1 h to evaporate any residual solvent.

2.3. Synthesis of GDLs. A custom-built CVD reactor with a square bottom of 31.6 cm in length and 4 cm in height was used for the fabrication of copolymer GDLs. The top of the reactor was covered with a 2.5 cm thick quartz plate. A filament array (80% Ni/20% Cr, AWG 26) suspended 2.5 cm above the bottom of the reactor was resistively heated to the desired temperature. Filament temperature was controlled via a thermocouple (type K, Omega Engineering) connected to a PID (proportional integral derivative) controller (model SSRL24ODC25, Omega Engineering). The substrate temperature was controlled by an external circulator (WiseCircu—refrigerated bath circulator) connected to the bottom part of the reactor. The pressure inside the reactor was adjusted with a throttling butterfly valve (model 253B, MKS type) and a pressure sensor (MKS 627D11TDC1B). Vacuum was provided with a rotary vane pump (BSV10, Baosi) with a cold trap attached on the exhaust line. Poly(V4D4), poly(PFHEA), and poly(PFEMA) homopolymers and their poly(V4D4-*co*-PFHEA) and poly(V4D4-*co*-PFEMA) copolymers were deposited on the crystalline silicon (c-Si) wafer, on 9.5 μm thick Psf support membranes for oxygen and WVP tests and on commercial GDEs (Ocali A.S.) after their original

https://doi.org/10.1021/acs.iecr.1c04244
Ind. Eng. Chem. Res. 2022, 61, 2633−2642

Table 1. Summary of Process Conditions for iCVD GDLs

sample name	F_{V4D4} (sccm)	F_{PFHEA} (sccm)	F_{PFEMA} (sccm)	F_{TBPO} (sccm)	P_{total} (mTorr)	$T_{substrate}$ (°C)	$T_{filament}$ (°C)	deposition rate (nm min^{-1})
V4D4 homopolymer	0.32			0.16	250	45	300	6.13
HCO-1	0.22	0.044		0.44		45		3.84
HCO-2		0.088						4.37
HCO-3		0.132			250		300	5.75
HCO-4		0.176						6.84
HCO-5		0.22						9.78
PFHEA homopolymer		0.32		0.11	250	25	300	89.87
ECO-1	0.22		0.044	0.44		45		2.64
ECO-2			0.088					2.85
ECO-3			0.132		250		300	3.11
ECO-4			0.176					3.29
ECO-5			0.22					3.72
PFEMA homopolymer			0.2	0.025	250	35	250	18.82

GDLs were removed for electrochemical characterization. Fluorinated monomers PFHEA and PFEMA in stainless steel containers were heated to 65 and 95 °C, respectively. Monomer vapors were metered into the chamber through a mass-flow controller (MFC) (model 1479A, MKS). TBPO was kept at room temperature and delivered to the reactor through an MFC (model 1479A, MKS). The V4D4 monomer was heated to 90 °C and fed into the chamber through a special MFC (model 1150C, MKS). Reactor pressure was maintained at 250 mTorr throughout the study. The substrate and filament temperatures were adjusted for the optimum deposition rate for homopolymers and copolymers. The filament temperature was set to 250 °C for the PFEMA homopolymer and fixed at 300 °C for all other homopolymer and copolymer film depositions. A final film thickness of 350 ± 50 nm was targeted.

2.4. Characterization of GDLs. Fourier transform infrared spectroscopy (FTIR) analysis was performed using a PerkinElmer Inc.-Spectrum BX FTIR spectrometer to investigate the quality and chemical composition of fabricated GDLs. The spectra were measured from 4000 to 650 cm^{-1} with a 4 cm^{-1} step size accumulating 20 scans. All spectra were baseline corrected and thickness normalized. Peak deconvolutions were performed using C═O stretching band in PFHEA and PFEMA (1700−1770 cm^{-1}) and asymmetric Si−O−Si stretching band (1010−1100 cm^{-1}) in V4D4 for chemical composition evaluation. The thickness measurements for iCVD-deposited GDLs were performed using an Mprobe-Vis20 reflectometer with the spectral range of 400−1100 nm and TF Companion software. The surface morphologies of GDLs were investigated using an FEI Quanta250 scanning electron microscopy (SEM) system with a field emission gun. A theta optical tensiometer system was used for water contact angle (WCA) measurements to investigate the hydrophobicity of the surface. Static contact angle measurements were performed by dropping 5 μL ultrapure water on the film surface. Water vapor transmission rates (WVTRs) of poly(V4D4), poly(PFHEA), and poly(PFEMA) homopolymers and their copolymers and Psf support membranes were determined using a Mocon Permatran-W model 3/33 instrument. Measurements were performed at 37.8 °C and at 90% relative humidity with a 100 cm^3 min^{-1} nitrogen flow rate, as described in ASTM F1249 standard. Permeance and permeability were calculated using eqs 1 and 2

$$\text{permeance} = \frac{\text{WVTR}}{S(R_1 - R_2)} \quad (1)$$

$$\text{permeability} = \text{permeance} \times \text{thickness} \quad (2)$$

where R_1 = relative humidity at the source expressed as a fraction (R_1 = 1.00 for a 100% RH chamber, and for 90% RH chamber, R_1 = 0.90). R_2 = relative humidity of the vapor sink expressed as a fraction [R_2 = 0 for the 0% RH chamber (dry side)]. S = vapor pressure of water at the test temperature.

Oxygen permeability measurements of iCVD-deposited homopolymers and copolymer films were performed on Psf support membranes following ASTM D3985 standard using a Dansensor Lyssy L-100-5000 manometric gas permeability tester. Measurements were performed at 23 °C and 0% relative humidity with a 5−10 cm^3 min^{-1} pure oxygen gas flow rate. Gas transmission rates for samples were calculated using eq 3

$$\frac{L}{P} = \frac{L_s}{P_s} + \frac{L_c}{P_c} \quad (3)$$

where P is the apparent permeability of the structure, L is the total thickness $L_s + L_c$, and P_s and P_c are the permeability of support (s) and coating (c), respectively.[30,31]

2.5. Fabrication of GDEs. Commercial GDEs used in this study consist of three parts: a catalyst layer, nickel mesh as a current collector, and a GDL. GDLs of commercially available GDEs were carefully removed without damaging catalyst layers and nickel current collectors. Poly(V4D4), poly(PFHEA), and poly(PFEMA) homopolymers and their poly(V4D4-*co*-PFHEA) and poly(V4D4-*co*-PFEMA) copolymers were deposited via iCVD to serve as GDLs only on the surface facing outside.

2.6. Electrochemical Measurements. All electrochemical measurements were performed using a potentiostat/galvanoostat/ZRA (Gamry model 22162) with tripolar electrode measurement apparatus. Electrochemical tests were performed in a custom-made three-electrode cell with 6 M KOH as the electrolyte, a Pt wire as the counter electrode, and a saturated Ag//AgCl reference electrode at 25 ± 2 °C. GDEs (8 mm in diameter) with iCVD GDLs (V4D4, PFHEA, or PFEMA homopolymers and their copolymers) were used as working electrodes. Measurements were carried out after 15 min N_2 purge and under a constant potential mode similar to previous studies in the literature.[32,33] Cyclic voltammetry (CV) was carried out between −0.8 and 1.2 V at a scan rate of 5 mV s^{-1}. AC impedance measurements of half-cells were also

https://doi.org/10.1021/acs.iecr.1c04244
Ind. Eng. Chem. Res. 2022, 61, 2633−2642

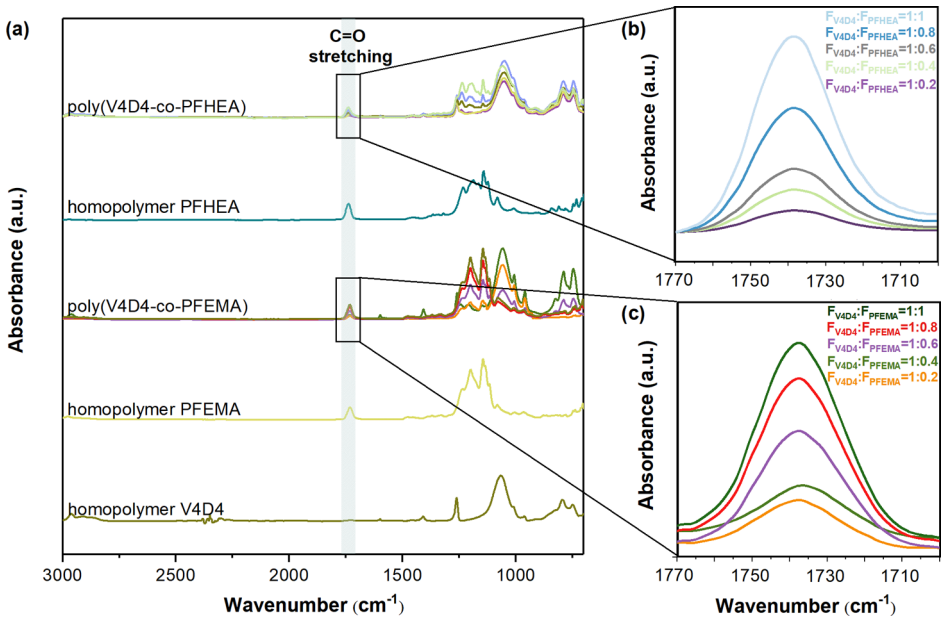

Figure 1. FTIR spectra of (a) V4D4, PFHEA, and PFEMA homopolymers and their copolymers, (b,c) enlargement of C=O stretching region for poly(V4D4-*co*-PFHEA) and poly(V4D4-*co*-PFEMA) copolymers, respectively.

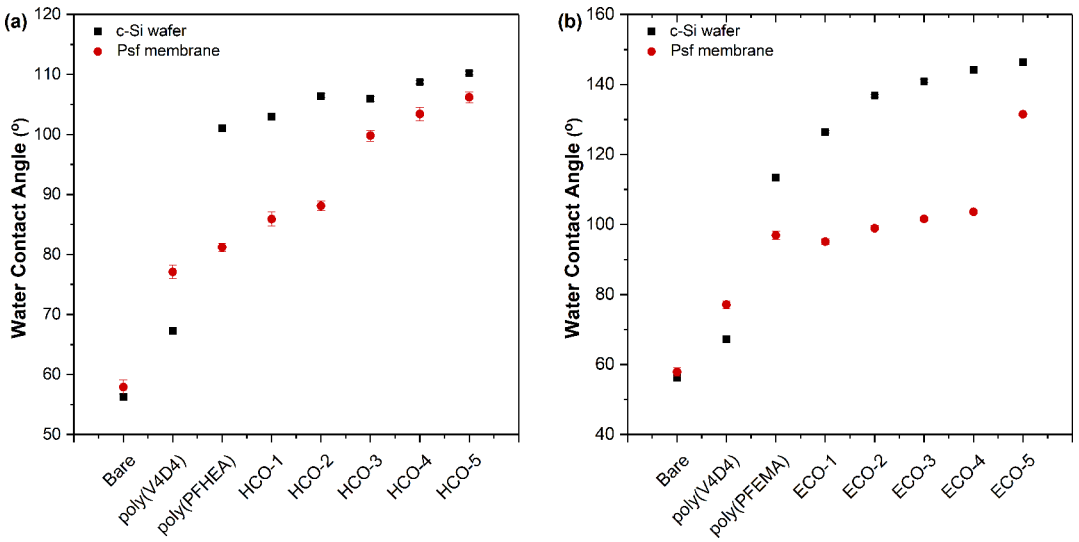

Figure 2. WCA measurements of iCVD poly(V4D4), (a) poly(PFHEA) and (b) poly(PFEMA) and their copolymers.

performed from 10 kHz to 10^{-1} Hz at room temperature. All electrochemical measurements were carried out under atmospheric conditions. Chronoamperometry (CA) measurements were performed at 1.5 V to evaluate diffusion coefficients.

3. RESULTS AND DISCUSSION

Two different series of copolymer films containing a highly oxygen permeable V4D4 and hydrophobic PFHEA and PFEMA were fabricated as GDLs via iCVD. Copolymer films with various fluorinated monomer (PFHEA or PFEMA):V4D4 ratios were obtained by adjusting the flow rates of monomers during polymerization. Similar deposition conditions reported in our previous work were used for iCVD GDL fabrication, as summarized in Table 1.[34]

In iCVD process, the deposition rate of polymers strongly depends on the concentration of adsorbed monomers on the substrate surface.[35,36] In case of copolymerization, at a fixed substrate temperature, the surface concentrations of monomers will vary depending on their partial vapor pressures on the gas phase and their saturation pressures (Supporting Information Figure S1). Therefore, the copolymer composition was controlled by adjusting the flowrates of monomers during polymerization. FTIR measurements were performed for all homo and copolymer films to evaluate the chemical composition of copolymers and cross-linking between vinyl groups in V4D4 and acrylic groups in fluoropolymers (Supporting Information Table S1). Figure 1 shows the FTIR spectra of homo and copolymer films deposited via iCVD. Figure 1b,c shows the enlargements of a portion of Figure 1a, emphasizing the absorption peaks ranging from 1700 to 1770 cm^{-1}. This enlarged view provides vital information about the changes in relative intensities of absorption peaks related to the C=O stretching in acrylic

https://doi.org/10.1021/acs.iecr.1c04244
Ind. Eng. Chem. Res. 2022, 61, 2633−2642

Table 2. Oxygen Permeability, WVP, WVTR, and Selectivity of Psf Support Membranes, Poly(V4D4), Poly(PFHEA), and Poly(PFEMA) Homopolymers and Their Copolymers[a]

	oxygen permeability $\times 10^{15}$ mol m m^{-2} s^{-1} Pa^{-1}	WVP $\times 10^{15}$ mol m m^{-2} s^{-1} Pa^{-1}	WVTR $\times 10^{-1}$ g m^{-2} day^{-1}	selectivity, α_{O_2/H_2O}
Psf support membrane	0.5	3.38 $\times 10^{6}$	98.4	1.47 $\times 10^{-7}$
poly(V4D4)	1.801 ± 0.288	0.412 ± 0.011	1.186 ± 0.063	4.36
poly(PFHEA)	0.204 ± 0.048	0.327 ± 0.001	0.686 ± 0.111	0.62
HCO-1	0.741 ± 0.007	0.475 ± 0.031	1.132 ± 0.134	1.56
HCO-2	1.162 ± 0.229	0.379 ± 0.038	0.859 ± 0.184	3.06
HCO-3	1.414 ± 0.205	0.345 ± 0.007	0.818 ± 0.039	4.09
HCO-4	1.895 ± 0.009	0.283 ± 0.001	0.673 ± 0.073	6.71
HCO-5	3.531 ± 0.761	0.268 ± 0.008	0.592 ± 0.073	13.16
poly(PFEMA)	0.608 ± 0.023	0.339 ± 0.006	0.461 ± 0.011	1.79
ECO-1	1.243 ± 0.228	0.581 ± 0.026	0.807 ± 0.029	2.14
ECO-2	1.146 ± 0.232	0.426 ± 0.025	0.684 ± 0.009	2.69
ECO-3	0.772 ± 0.139	0.363 ± 0.006	0.709 ± 0.041	2.13
ECO-4	1.072 ± 0.188	0.353 ± 0.007	0.634 ± 0.033	3.03
ECO-5	1.125 ± 0.139	0.261 ± 0.004	0.548 ± 0.061	4.33

[a]Selectivity (α_{O_2/H_2O}) is described as $\alpha_{O_2/H_2O} = P_{O_2}/P_{H_2O}$ (the unit of permeability is mol m m^{-2} s^{-1} Pa^{-1}).[24] 1 Barrer = 3.35 $\times 10^{-16}$ mol m m^{-2} s^{-1} Pa^{-1}.

groups for copolymers with increasing PFHEA and PFEMA contents. The fluorinated monomer fraction in copolymers is directly related to area of this individual peak. As expected, the highest peak intensity (and peak area) was observed when the fluorinated monomer/V4D4 flow rate ratio is 1 and decreases with increasing V4D4 in the copolymer composition.

A GDL in an alkaline metal−air battery should have low water/electrolyte permeability to prevent corrosion of the metal anode by moisture. Especially in a humid environment, water uptake by GDE leads to reduced electrochemical activity and ionic conductivity due to dilution of the electrolyte.[5,6,15,16,37] Therefore, an ideal GDL should be superhydrophobic, have high oxygen permeability, and exhibit very low water permeability. Figure 2 shows WCA measurements performed on iCVD copolymer films fabricated on c-Si and Psf support membranes. Higher contact angles for poly(V4D4-*co*-PFHEA) copolymers compared to the poly(PFHEA) homopolymer on bare Psf membrane (57.96 ± 1.15°) and bare Si wafer (56.25 ± 1.15°) are mainly due to the existence of fluorinated groups in PFHEA. As expected, WCA values increase with the increase in fluorinated groups in the copolymer composition. In addition, an increase in the surface roughness of copolymer films can also contribute to hydrophobicity.[35,38] WCA of the poly(PFEMA) homopolymer on the Si wafer and Psf membrane measured as 145.4 ± 0.3 and 131.5 ± 0.4°, respectively, are significantly higher than that of the poly(PFHEA) homopolymer, as seen in Figure 2b. Interestingly, WCA values of poly(V4D4-*co*-PFEMA) copolymers did not show a significant change on the Psf support membrane but showed considerable changes on the c-Si substrate as the PFEMA/V4D4 ratio increased. In addition, the WCA value of the poly(V4D4) homopolymer on the Psf support membrane was found to be higher than the WCA value on c-Si. This can be attributed to the roughness of the Psf membrane surface (Supporting Information Figure S2).[39]

WCA measurements are consistent with surface free energies reported in the literature, and there is a significant difference in surface energies between the V4D4 monomer (36.6 mJ m^{-2}) and fluorinated PFHEA and PFEMA (10.5 and 6−8 mJ m^{-2}, respectively) monomers, making them immiscible to each other (see Supporting Information Table S2). However, in the iCVD process, these monomers are vaporized and mixed in the vapor phase where the effect of surface tension is very small before actual polymerization occurs on the substrate surface. Therefore, iCVD enables the fabrication of homogenous films without phase segregation problems.[35] In a metal−air battery, the water intake through the GDE should be minimum for electrochemical stability. Electrode corrosion and capacity loss due to water are serious problems, especially for alkaline metal−air batteries. Since iCVD-fabricated GDLs were very thin (~300−400 nm), Psf membranes were used to mechanically support homo and copolymer iCVD films during WVP measurements. The as-prepared Psf support membranes have a water permeability of 3.38 $\times 10^{-9}$ mol m m^{-2} Pa^{-1} s^{-1} and a WVTR approximately 9.84 $\times 10^{2}$ g m^{-2} day^{-1}, making Psf a very suitable support material to measure the oxygen and water permeabilities of iCVD-fabricated GDLs.[28,40] WVP and WVTR values of poly(V4D4), poly(PFHEA), and poly(PFEMA) homopolymers and their copolymers are given in Table 2.

Commercially available thick GDLs that are used in fuel-cells and metal−air batteries exhibit WVTRs between 11.16 and 811.99 g m^{-2} day^{-1}.[5,6,16] WVTRs for poly(V4D4-*co*-PFHEA) and poly(V4D4-*co*-PFEMA) copolymers varied between 5.48 and 11.32 g m^{-2} day^{-1}; between 2 and 150 times lower than commercial GDLs. Increasing fluorinated monomers in the copolymer composition resulted in a slight reduction in WVP. HCO and ECO series GDLs showed comparable WVPs; however, a clear trend of decreasing WVP with increasing fluorinated monomers was observed for both series. The role of a GDL is to provide sufficient oxygen transfer from air to catalyst layers in GDEs while limiting the water intake from ambient. In the literature, perfluorinated chemicals were used as oxygen-selective membranes[15,16] or electrolyte additives[41,42] in Li−O_2 batteries. Most commercially available GDLs used in alkaline metal−air batteries are thick and highly porous membranes or non-woven polymeric materials with hydrophobic outer surface, exhibiting very high oxygen and WVPs. Reported oxygen permeabilities of thin film non-porous polymeric GDLs such as PET, high density polyethylene (HDPE), and polytetrafluoroethylene (PTFE) prepared via extrusion or other methods and thicknesses

https://doi.org/10.1021/acs.iecr.1c04244
Ind. Eng. Chem. Res. 2022, 61, 2633−2642

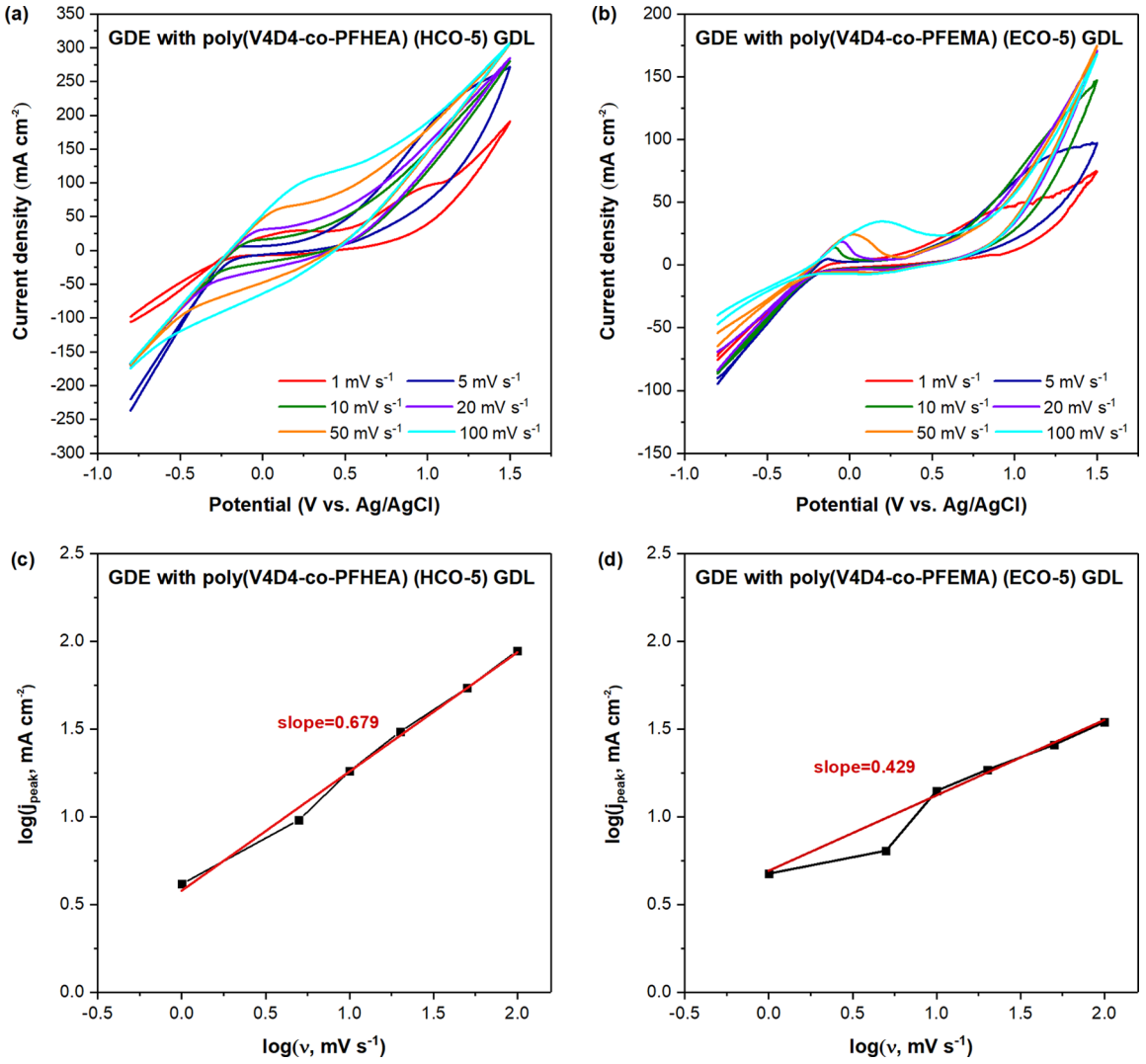

Figure 3. Effect of the voltametric scan rate on current density for GDEs with (a) HCO-5 and (b) ECO-5 GDLs and (c,d) corresponding relation of logarithm of peak current and logarithm of the scan rate.

between 10 and 1000 μm vary between 3.35×10^{-18} mol m m^{-2} s^{-1} Pa^{-1} (0.01 Barrer) and 3.35×10^{-15} mol m m^{-2} s^{-1} Pa^{-1} (10 Barrer).[27] For comparison, very thin (350 ± 50 nm) iCVD prepared homo and copolymer films showed oxygen permeabilities, ranging from 0.204×10^{-15} to 1.895×10^{-15} mol m m^{-2} s^{-1} Pa^{-1} (from 0.61 to 5.66 Barrer) except for the poly(V4D4-*co*-PFHEA) copolymer with a 1:1 ratio of V4D4:PFHEA having the highest oxygen permeability of 3.53×10^{-15} mol m m^{-2} s^{-1} Pa^{-1} (10.5 Barrer) (Supporting Information Figure S3). Fluorinated homopolymers exhibit lower oxygen permeabilities compared to the poly(V4D4) homopolymer; however, oxygen permeability increases with the addition of PFHEA in HCO series. A similar trend is not observed for ECO series. The poly(PFEMA) homopolymer exhibited higher oxygen permeability than the poly(PFHEA) homopolymer. Oxygen permeability and WVP seem to be inversely related due to the higher water diffusion rate and smaller molecule size compared to oxygen.[5,42] In theory, the performance of GDEs should increase using iCVD-deposited copolymer GDLs due to enhanced oxygen and reduced water permeabilities compared to conventional GDEs with relatively thick fluoropolymer GDLs. Poly(V4D4-*co*-PFHEA) copolymer (HCO-5) showed 17 times increase in oxygen permeability with more than 1.2 times lower water permeability (corresponding to an oxygen/water selectivity of 13.6) compared to the poly(PFHEA) homopolymer. Poly(V4D4-*co*-PFEMA) copolymers did not show such drastic changes in oxygen and water permeabilities. These observations suggest that poly(V4D4-*co*-PFHEA) copolymers are promising water barriers with enhanced oxygen permeabilities as GDLs.

Electrochemical properties of GDEs prepared with iCVD copolymer GDLs were evaluated by CV measurements with GDL exposed to air and the other side in contact with 6 M KOH solution. The area of GDE in contact with the solution was 0.502 cm^2. Figure 3 shows the effect of the scan rate on the electrochemical behavior of GDEs with poly(V4D4-*co*-PFHEA) (HCO-5) and poly(V4D4-*co*-PFEMA) (ECO-5) GDLs only. The peak related to oxygen reduction reactions can be observed in a wide potential range from −0.8 to 1.2 V. Therefore, the voltage range of −0.8−1.2 V was selected during CV measurements.

The power-law dependence of the current density on the scan rate can be expressed by the following equation[43]

$$\log j = b \log \nu + \log a \quad (4)$$

https://doi.org/10.1021/acs.iecr.1c04244
Ind. Eng. Chem. Res. 2022, 61, 2633−2642

where j is current density, ν represents the scan rate, and a is a constant. The slope, b, describes the charge-transfer coefficient; a value close to 0.5 indicates a diffusion-controlled process, whereas values close to 1 indicate the pseudocapacitive case, in which faradaic charge transfer occurs by intercalation or adsorption of charge-compensating ions. The oxidation peak current densities for GDEs with HCO-5 and ECO-5 GDLs increase with $\nu^{0.68}$ and $\nu^{0.43}$, respectively [$\log j_{peak} = 0.679 \log \nu + 0.706$ ($R^2 = 0.9939$) for HCO-5 and $\log j_{peak} = 0.429 \log \nu + 0.692$ ($R^2 = 0.9955$) for ECO-5 GDL]. It seems the performance of both GDEs are mass transport limited.[44] Especially at higher scan rates, the charge flow decreases with the increasing scan rate. Oxidation peaks for GDEs with poly(V4D4-*co*-PFHEA) and poly(V4D4-*co*-PFEMA) GDLs were more obvious at high scan rates. The peak was detected at a potential of 0.9 V related to the 2 + 2-electron reduction reaction. The increase in peak broadening was observed when the scan rate is increased from 1 to 5 mV s^{-1}. Additionally, there was a positive shift of peak potentials with the increasing scan rate.[45] The peak broadening was not observed in higher scan rates since the peak was out of range due to the peak position shift.

CV curves of the samples at a 5 mV s^{-1} sweep rate are shown in Figure 4. The onset potential for oxygen evolution

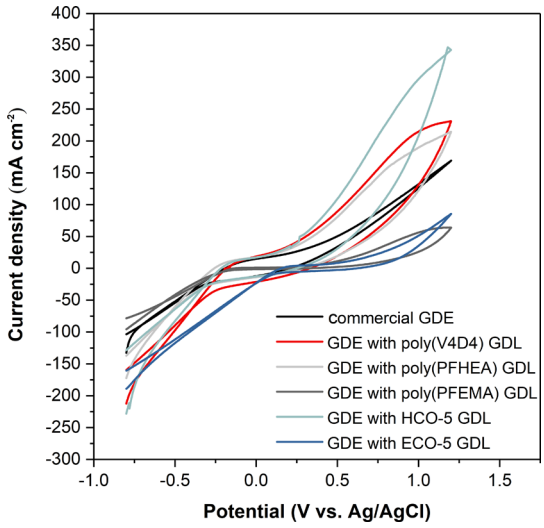

Figure 4. Cyclic voltammograms of GDEs with iCVD GDLs between −0.8 and 1.2 V with a sweep rate of 5 mV s^{-1}.

took place at 0.3 V vs Ag//AgCl, whereas the onset potential of oxygen reduction was below −0.2 V. The GDE with HCO-5 GDL showed a higher current density when compared to commercial GDEs with conventional thick GDLs. The increase in current density is due to higher oxygen transport in copolymer GDLs. A lower reduction current density was observed for GDEs with ECO-5 GDL (189.2 mA cm^{-2}) when compared to GDEs with HCO-5 GDL (228.2 mA cm^{-2}) at −0.8 V. These observations are in good agreement with the oxygen and water permeability results, considering especially high oxygen permeability of HCO-5 GDL. In addition, stability of GDEs is also an important parameter for evaluating the battery performance. Therefore, long-term stability tests of GDEs with HCO-5 GDLs were performed (Supporting Information Figure S4). It was observed that GDEs with HCO-5 GDL were more stable for oxygen reduction reaction (ORR) activity and did not show a significant change in current density after 240 h immersion in 6 M KOH electrolyte. Tafel slopes calculated from Tafel plots also confirmed the results (Supporting Information Figures S5, S6 and Table S3).

Electrochemical impedance spectroscopy (EIS) is a powerful tool to characterize impedances in a GDE. EIS analysis was performed at the open-circuit potential from 10 kHz to 10^{-1} Hz in 6 M KOH solution. Nyquist plots, as shown in Figure 5a, provide information on three types of GDE resistances; ohmic (solution), charge transfer, and diffusion resistances.[33] Nyquist plots of GDEs consist of a single semi-circular curve and a diffusion drift, which can be fitted using the Randles and equivalent circuit model, as shown in Figure 5b. The Randles model (model 1) is generally used to describe simple electrochemical systems and includes only electrolyte resistance (R_e), charge-transfer resistance (R_{ct}) in the medium-frequency region, and Warburg impedance (Z_W) in the low-frequency region. The Warburg impedance is expressed as $Z_W = \sigma_w\omega^{-1/2} - j\sigma_w\omega^{-1/2}$ ($j^2 = -1$) and $Z_W = W^{-1}/\sqrt{j\omega}$ where σ_w represents the Warburg impedance coefficient ($\Omega \cdot s^{1/2}$), ω is the angular frequency ($\omega = 2\pi f$), and W is Warburg impedance element (S $s^{1/2}$).[46] The Warburg impedance coefficient is related to the diffusion coefficient, and lower σ_w values indicate faster diffusion. In the high-frequency region, the intercept in x-axis (Z_{real}) represents the ohmic (electrolyte) resistance (R_e), and the semicircle from high- to medium-frequency range is associated with the combination of charge-transfer resistance (R_{ct}) and interfacial resistance (R_f). Model 2 expands model 1 with the addition of interfacial resistance (R_f). Electrochemical parameters extracted from the fit to the equivalent circuit models are listed in Table 3. R_{ct} and R_f describe the kinetics of the cell reaction. Lower values of R_{ct} and R_f indicate faster reaction kinetics.[47] As listed in Table 3, the GDE with poly(V4D4) homopolymer GDL shows at least 4 orders of magnitude higher charge-transfer resistance than other GDEs. The lowest value of $R_{ct} + R_f$ was obtained with HCO-5 GDL (1.50 + 2.89 Ω), which is consistent with Nyquist plots, as seen in Figure 5a. For commercial GDEs, W value describing the diffusion at the interface between the electrolyte and active material particles was determined to be 0.81. GDEs with poly(V4D4) GDL and HCO-5 GDL exhibited higher W values (0.92 and 0.84, respectively) than commercial GDEs, indicating better oxygen transport.

The relation between real impedance (Z_{re}) and angular frequency (ω) in the low-frequency region is shown using the following equation.[48,49]

$$Z_{re} = R_e + R_{ct} + \sigma_w\omega^{-1/2} \quad (5)$$

$$D = R^2T^2/2A^2n^4F^4C^2\sigma_w^2 \quad (6)$$

where D is the diffusion coefficient (cm^2 s^{-1}), R is the gas constant, T is the temperature (K), F is the Coulomb constant (96,485 C mol^{-1}), A is GDE area (cm^2), n is the number of electrons per molecule, C is the molar concentration ion (mol m^{-3}), and σ_w is the Warburg impedance coefficient (Ω $s^{-1/2}$). The Warburg impedance coefficient (σ_w) of GDEs with HCO-5 GDL (0.32) is lower than that of commercial GDEs (0.37), indicating better diffusion, as listed in Table 3.

For comparison, oxygen transport was also evaluated by chronoamperometric method which is a useful tool to evaluate diffusion coefficients. Oxygen transport process in the electrode takes place in three steps: (i) oxygen diffusion

https://doi.org/10.1021/acs.iecr.1c04244
Ind. Eng. Chem. Res. 2022, 61, 2633−2642

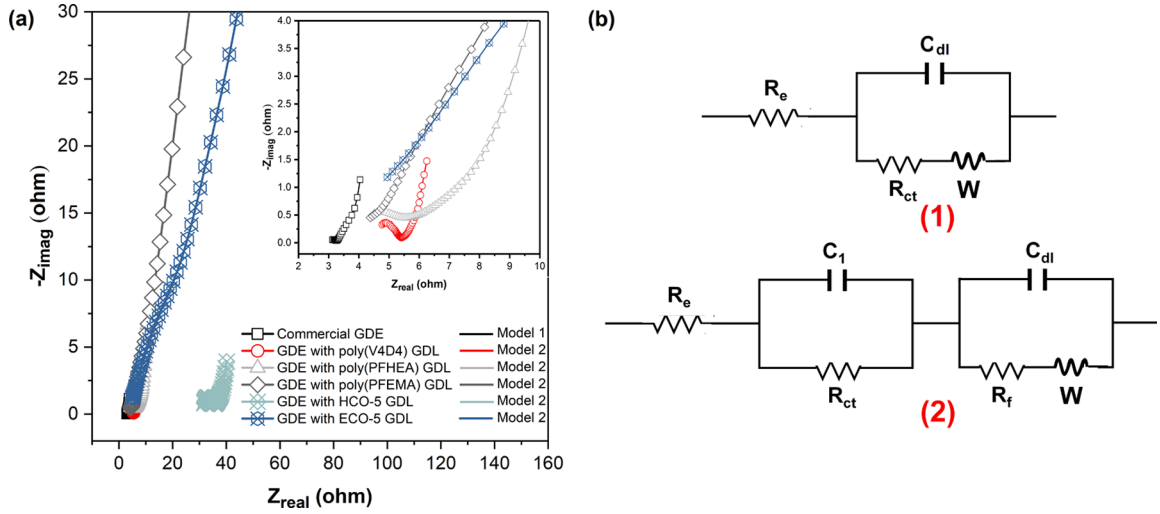

Figure 5. (a) Impedance spectra of GDEs, (b) equivalent electrical circuit models [(1) model 1 and (2) model 2. Resistances (R_i), double-layer capacitance (C_{dl}), Warburg impedance (W), electrolyte resistance (R_e), and capacitance of the film (C_i)].

Table 3. Electrochemical Parameters Extracted from the Fit to the Equivalent Circuit Models for EIS Data

sample	R_e, Ω	R_{ct}, Ω	R_f, Ω	W, S $s^{1/2}$	chi-square, χ^2	Warburg impedance coefficient, σ_w, Ω·$s^{-1/2}$
commercial GDE	3.55	0.14		0.81	0.8×10^{-4}	0.37
GDE w/poly(V4D4) GDL	4.67	6.55×10^{4}	0.71	0.92	1.84×10^{-4}	0.29
GDE w/poly(PFHEA) GDL	4.32	4.12	0.89	0.16	9.72×10^{-4}	1.52
GDE w/poly(PFEMA) GDL	4.84	4.42	0.68	0.79	4.1×10^{-4}	9.99
GDE w/HCO-5 GDL	32	1.50	2.89	0.84	5.53×10^{-5}	0.32
GDE w/ECO-5 GDL	4.85	3.28	7.79	1.5×10^{-2}	4.39×10^{-3}	12.32

across GDL, (ii) dissolution of oxygen into the electrolyte film which create three-phase (gas-liquid-solid) boundary, (iii) diffusion of the dissolved oxygen through thin film to reactive site. Using the Cottrell equation[50,51]

$$i(t) = nFAC^* \sqrt{\left(\frac{D}{\pi t}\right)} \quad (7)$$

where i is the limited current (A), n the number of electrons, F the Columb constant (96,485 C mol^{-1}), A the surface area of the electrode (cm^2), D the diffusion coefficient (cm^2 s^{-1}), t the time (s) and C^* is the concentration of reactant (M), oxygen diffusion coefficients for different samples can be calculated. The diffusion process is slow and dependent on the thickness of GDL; therefore, using ultra-thin iCVD GDLs should improve oxygen mass transport.[51] Oxygen diffusion coefficients listed in Table 4 were calculated using EIS (eq 6) and CA (eq 7) data for comparison. Although there are small differences in calculated diffusion coefficients between two methods, the results agree well with oxygen permeability measurements. The oxygen diffusion coefficient of poly(PFHEA) homopolymer GDLs is comparable to oxygen diffusion coefficient of commercial GDE. The oxygen diffusion coefficient for the GDE with HCO-5 GDL in 6 M KOH solution is 20 times higher than that for commercial GDE and is almost 4 times higher than GDE with ECO-5 GDL making it a better candidate as GDL for use in a GDE for a metal−air battery. Poly(V4D4-*co*-PFHEA) copolymer GDLs improve the oxygen transport due to a cross-linked network structure with the highly oxygen permeable siloxane and smaller fluorinated groups compared to poly(V4D4-*co*-PFEMA).

Table 4. Calculated Oxygen Diffusion Coefficients for GDEs

GDEs	diffusion coefficient × 10^8, cm^2 s^{-1} (using EIS data)	diffusion coefficient × 10^8, cm^2 s^{-1} (using CA data)
commercial GDE	1.69	1.84
GDE w/poly(V4D4) GDL	26.8	22.5
GDE w/poly(PFHEA) GDL	2.32	3.94
GDE w/poly(PFEMA) GDL	0.23	0.28
GDE w/HCO 5 GDL	32.5	39.51
GDE w/ECO 5 GDL	8.64	6.76

4. CONCLUSIONS

Poly(V4D4), poly(PFHEA), poly(PFEMA) homopolymer, poly(V4D4-*co*-PFHEA), and poly(V4D4-*co*-PFEMA) copolymer coatings with different compositions were deposited via iCVD as GDLs on GDEs for metal−air batteries. Oxygen permeability and WVP of GDLs (350 ± 50 nm in thickness) were measured using 9.5 μm thick Psf support membranes. In the literature, WVTRs for GDLs for GDE were reported as 11.16−811.99 g m^{-2} day^{-1}.[5,6,16] It was found that thin iCVD GDLs exhibited WVTRs, varying from 5.48 to 11.32 g m^{-2} day^{-1}; between 2 and 150 times lower than commercial GDLs.[28] In addition, polymeric materials used as GDLs such as polyimide Kapton,[52] PVDF-HFP,[5] HDPE,[16] PTFE,[53] and so forth were reported have oxygen permeabilities between 0.01 and 4.21 Barrer. iCVD-deposited GDLs exhibited higher

https://doi.org/10.1021/acs.iecr.1c04244
Ind. Eng. Chem. Res. 2022, 61, 2633−2642

oxygen permeability, varying between 0.61 and 5.66 Barrer (0.204×10^{-15} and 1.895×10^{-15} mol m m^{-2} s^{-1} Pa^{-1}). The iCVD-deposited poly(V4D4-*co*-PFHEA) copolymer with a 1:1 ratio of V4D4/PFHEA showed an exceptional 10.5 Barrer (3.53×10^{-15} mol m m^{-2} s^{-1} Pa^{-1}), the highest oxygen permeability for similar GDLs reported in the literature. The electrochemical performance of GDEs with iCVD GDLs was investigated by polarization measurements, CV, and EIS analysis. CV analysis showed that poly(V4D4-*co*-PFHEA) GDLs are responsible for higher electrocatalytic activity for oxygen reduction compared to homopolymer and poly(V4D4-*co*-PFEMA) copolymer GDLs. Fabricated GDE electrodes with poly(V4D4-*co*-PFHEA) and poly(V4D4-*co*-PFEMA) exhibited higher oxygen reduction current densities (228.2 and 189.2 mA cm^{-2}, respectively) compared to commercial GDEs (132.7 mA cm^{-2}). The CA measurements and EIS analysis also confirmed the findings of oxygen permeability measurements. By combining siloxane and fluorinated polymer matrix, poly(V4D4-*co*-PFHEA) copolymer GDLs provide enhanced oxygen transport and reduce moisture entrance significantly. Using the well-balanced properties of siloxane and fluorinated polymer chemistries, the iCVD process is an excellent low-cost method for the fabrication of oxygen-permeable hydrophobic GDLs for battery applications.

■ ASSOCIATED CONTENT

Supporting Information

The Supporting Information is available free of charge at https://pubs.acs.org/doi/10.1021/acs.iecr.1c04244.

Effect of the monomer flow rate on the polymer deposition rate, FTIR analysis of iCVD GDLs, SEM analysis of iCVD GDLs, surface free energies of iCVD GDLs, oxygen permeabilities of GDLs, linear sweep voltammetry measurements, and Tafel plots of GDEs (PDF)

■ AUTHOR INFORMATION

Corresponding Author

Özgenç Ebil − *Faculty of Engineering, Department of Chemical Engineering, İzmir Institute of Technology, 35430 Izmir, Turkey;* orcid.org/0000-0002-7458-4219; Phone: +90 (232) 750 6616; Email: ozgencebil@iyte.edu.tr

Author

Gizem Cihanoğlu − *Faculty of Engineering, Department of Chemical Engineering, İzmir Institute of Technology, 35430 Izmir, Turkey*

Complete contact information is available at: https://pubs.acs.org/10.1021/acs.iecr.1c04244

Author Contributions

The manuscript was written through contributions of all authors. All authors have given approval to the final version of the manuscript.

Notes

The authors declare no competing financial interest.

■ ACKNOWLEDGMENTS

This work was partially supported by the Scientific and Technological Research Council of Turkey (TÜBİTAK) (grant number 114M233).

■ REFERENCES

(1) Clark, S.; Mainar, A. R.; Iruin, E.; Colmenares, L. C.; Blázquez, J. A.; Tolchard, J. R.; Jusys, Z.; Horstmann, B. Designing Aqueous Organic Electrolytes for Zinc-air Batteries: Method, Simulation, and Validation. *Adv. Energy Mater.* **2020**, *10*, 1903470.

(2) Linden, D.; Reddy, T. B. *Handbook of Batteries*, 3rd ed.; Mcgraw Hill: England, 2001.

(3) Schröder, D.; Laue, V.; Krewer, U. Numerical Simulation of Gas-Diffusion-Electrodes with Moving Gas-Liquid Interface: A Study on Pulse-Current Operation and Electrode Flooding. *Comput. Chem. Eng.* **2016**, *84*, 217−225.

(4) Ikezawa, A.; Seki, K.; Arai, H. Design of Bifunctional Air Electrodes Based on the Reaction Fields between Oxygen Reduction Reaction and Oxygen Evolution Reaction. *Electrochim. Acta* **2021**, *394*, 139128.

(5) Amici, J.; Francia, C.; Zeng, J.; Bodoardo, S.; Penazzi, N. Protective PVDF-HFP-based Membranes for Air De-hydration at the Cathode of the Rechargeable Li-air Cell. *J. Appl. Electrochem.* **2016**, *46*, 617−626.

(6) Amici, J.; Alidoost, M.; Francia, C.; Bodoardo, S.; Martinez Crespiera, S.; Amantia, D.; Biasizzo, M.; Caldera, F.; Trotta, F. O_2 Selective Membranes Based on a Dextrin-Nanosponge (NS) in a PVDF-HFP Polymer Matrix for Li-air Cells. *Chem. Commun.* **2016**, *52*, 13683−13686.

(7) Mainar, A. R.; Iruin, E.; Colmenares, L. C.; Kvasha, A.; de Meatza, I.; Bengoechea, M.; Leonet, O.; Boyano, I.; Zhang, Z.; Blazquez, J. A. An Overview of Progress in Electrolytes for Secondary Zinc-air Batteries and Other Storage Systems Based on Zinc. *J. Energy Storage* **2018**, *15*, 304−328.

(8) Crowther, O.; Meyer, B.; Morgan, M.; Salomon, M. Primary Li-air Cell Development. *J. Power Sources* **2011**, *196*, 1498−1502.

(9) Kim, J.; Park, H.; Lee, B.; Seong, W. M.; Lim, H.-D.; Bae, Y.; Kim, H.; Kim, W. K.; Ryu, K. H.; Kang, K. Dissolution and Ionization of Sodium Superoxide in Sodium Oxygen Batteries. *Nat. Commun.* **2016**, *7*, 10670.

(10) Chang, Y.; Dong, S.; Ju, Y.; Xiao, D.; Zhou, X.; Zhang, L.; Chen, X.; Shang, C.; Gu, L.; Peng, Z.; Cui, G. A Carbon- and Binder-Free Nanostructured Cathode for High-Performance Nonaqueous Li-O_2 Battery. *Adv. Sci.* **2015**, *2*, 1500092.

(11) Zhu, J.; Yang, J.; Zhou, J.; Zhang, T.; Li, L.; Wang, J.; Nuli, Y. A Stable Organic-inorganic Hybrid Layer Protected Lithium Metal Anode for Long-cycle Lithium-Oxygen Batteries. *J. Power Sources* **2017**, *366*, 265−269.

(12) Yang, X.-y.; Xu, J.-j.; Bao, D.; Chang, Z.-w.; Liu, D.-p.; Zhang, Y.; Zhang, X.-B. High Performance Integrated Self-Package Flexible Li-O_2 Battery Based on Stable Composite Anode and Flexible Gas Diffusion Layer. *Adv. Mater.* **2017**, *29*, 1700378.

(13) Flegler, A.; Hartmann, S.; Settelein, J.; Mandel, K.; Sextl, G. Screen Printed Bifunctional Gas Diffusion Electrodes for Aqueous Metal-Air Batteries: Combining the Best of the Catalyst and Binder World. *Electrochim. Acta* **2017**, *258*, 495−503.

(14) Mainar, A. R.; Leonet, O.; Bengoechea, M.; Boyano, I.; de Meatza, I.; Kvasha, A.; Guerfi, A.; Blázquez, J. A. Alkaline Aqueous Electrolytes for Secondary Zinc-Air atteries: An Overview. *Int. J. Energy Res.* **2016**, *40*, 1032−1049.

(15) Ruan, Y.; Sun, J.; Song, S.; Yu, L.; Chen, B.; Li, W.; Qin, X. A Perfluorocarbon−Silicone Oil Oxygen−Selective Membrane for Ambient Operation of Aprotic Li−air Batteries. *Electrochem. Commun.* **2018**, *96*, 93−97.

(16) Xie, M.; Huang, Z.; Lin, X.; Li, Y.; Huang, Z.; Yuan, L.; Shen, Y.; Huang, Y. Oxygen Selective Membrane Based on perfluoropolyether for Li-air Battery with Long Cycle Life. *Energy Storage Mater.* **2019**, *20*, 307−314.

(17) Wang, N.; Han, Z.; Cao, X.; Fu, J.; Chen, Y.; Xiong, D. Designing Long-Term Cycle Life for a Lithium-Air Battery with a Modified Gas Diffusion Layer in Terms of the Moisture Intrusion and Electrolyte Volatilization. *J. Phys. Chem. C* **2021**, *125*, 24787−24795.

(18) Lin, G.; Nguyen, T. V. Effect of Thickness and Hydrophobic Polymer Content of the Gas Diffusion Layer on Electrode Flooding Level in a PEMFC. *J. Electrochem. Soc.* **2005**, *152*, A1942−A1948.
(19) Zhang, G. Q.; Zheng, J. P.; Liang, R.; Zhang, C.; Wang, B.; Hendrickson, M.; Plichta, E. J. Lithium-Air Batteries Using SWNT/CNF Buckypapers as Air Electrodes. *J. Electrochem. Soc.* **2010**, *157*, A953−A956.
(20) Fu, Z.; Wei, Z.; Lin, X.; Huang, T.; Yu, A. Polyaniline Membranes as Waterproof Barriers for Lithium-air Batteries. *Electrochim. Acta* **2012**, *78*, 195−199.
(21) Zhang, J.; Xu, W.; Liu, W. Oxygen-Selective Immobilized Liquid Membranes for Operating of Lithium-Air Batteries in Ambient Air. *J. Power Sources* **2010**, *195*, 7438−7444.
(22) Qi, Z.; Lefebvre, M. C.; Pickup, P. G. Electron and Proton Transport in Gas Diffusion Electrodes Containing Electronically Conductive Proton-Exchange Polymers. *J. Electroanal. Chem.* **1998**, *459*, 9−14.
(23) Antolini, E.; Giorgi, L.; Pozio, A.; Passalacqua, E. Influence of Nafion Loading in the Catalyst Layer of Gas-Diffusion Electrodes for PEFC. *J. Power Sources* **1999**, *77*, 136−142.
(24) Cao, L.; Lv, F.; Liu, Y.; Wang, W.; Huo, Y.; Fu, X.; Sun, R.; Lu, Z. A High Performance O_2 Selective Membrane Based on CAU-1-NH_2@Polydopamine and the PMMA Polymer for Li-Air Batteries. *Chem. Commun.* **2015**, *51*, 4364−4367.
(25) Zhang, J.; Xu, W.; Li, X.; Liu, W. Air Dehydration Membranes for Nonaqueous Lithium-Air Batteries. *J. Electrochem. Soc.* **2010**, *157*, A940.
(26) Labbe, M.; Clark, M. P.; Abedi, Z.; He, A.; Cadien, K.; Ivey, D. G. Atomic Layer Deposition of Iron Oxide on a Porous Carbon Substrate via Ethylferrocene and an Oxygen Plasma. *Surf. Coat. Technol.* **2021**, *421*, 127390.
(27) Crowther, O.; Salomon, M. Oxygen Selective Membranes for Li-air (O_2) Batteries. *Membranes* **2012**, *2*, 216−227.
(28) Choi, H.-g.; Shah, A. A.; Nam, S.-E.; Park, Y.-I.; Park, H. Thin-Film Composite Membranes Comprising Ultrathin Hydrophilic Polydopamine Interlayer with Graphene Oxide for Forward Osmosis. *Desalination* **2019**, *449*, 41−49.
(29) Ravishankar, H.; Christy, J.; Jegatheesan, V. Graphene Oxide (GO)-blended Polysulfone (Psf) Ultrafiltration Membranes for Lead Ion Rejection. *Membranes* **2018**, *8*, 77−90.
(30) Chatham, H. Oxygen Diffusion Barrier Properties of Transparent Oxide Coatings on Polymeric Substrates. *Surf. Coat. Technol.* **1996**, *78*, 1−9.
(31) Chen, Y.; Ye, Y.; Chen, Z.-R. Vapor-Based Synthesis of Bilayer Anti-Corrosion Polymer Coatings with Excellent Barrier Property and Superhydrophobicity. *J. Mater. Sci.* **2019**, *54*, 5907−5917.
(32) Yatagai, T.; Ohkawa, Y.; Kubo, D.; Kawase, Y. Hydroxyl Radical Generation in Electro-Fenton Process with a Gas-Diffusion Electrode: Linkages with Electro-Chemical Generation of Hydrogen Peroxide and Iron Redox Cycle. *J. Environ. Sci. Health, Part A: Environ. Sci. Eng. Toxic Hazard. Subst. Control* **2017**, *52*, 74−83.
(33) Tada, S.; Privatananupunt, P.; Iwasaki, T.; Kikuchi, R. Gas Diffusion Electrode with Large Amounts of Gas Diffusion Channel using Hydrophobic Carbon Fiber: For Oxygen Reduction Reaction at Gas/Liquid Interfaces. *J. Electrochem. Energy Convers. Storage* **2017**, *14*, 020903.
(34) Cihanoğlu, G.; Ebil, O. Robust Fluorinated Siloxane Copolymers via Initiated Chemical Vapor Deposition for Corrosion Protection. *J. Mater. Sci.* **2021**, *56*, 11970−11987.
(35) Kwak, M. J.; Oh, M. S.; Yoo, Y.; You, J. B.; Kim, J.; Yu, S. J.; Im, S. G. Series of Liquid Separation System Made of Homogeneous Copolymer Films with Controlled Surface Wettability. *Chem. Mater.* **2015**, *27*, 3441−3449.
(36) Gleason, K. K. *CVD Polymer: Fabrication of Organic Surfaces and Devices*, 1st ed.; Wiley-VCH: Germany, 2015.
(37) Mladenova, E.; Slavova, M.; Mihaylova-Dimitrova, E.; Burdin, B.; Abrashev, B.; Krapchanska, M.; Raikova, G.; Vladikova, D. Monolithic Carbon-Free Gas Diffusion Electrodes for Secondary Metal-Air Batteries. *J. Electroanal. Chem.* **2021**, *887*, 115112.
(38) Seok, J.-H.; Kim, S. H.; Cho, S. M.; Yi, G.-R.; Lee, J. Y. Crosslinked Organosilicon-Acrylate Copolymer Moisture Barrier Thin Film Fabricated by Initiated Chemical Vapor Deposition (iCVD). *Macromol. Res.* **2018**, *26*, 1257−1264.
(39) Nabe, A.; Staude, E.; Belfort, G. Surface Modification of Polysulfone Ultrafiltration Membranes and Fouling by BSA Solutions. *J. Membr. Sci.* **1997**, *133*, 57−72.
(40) Baldo, L. G. M.; Lenzi, M. K.; Eiras, D. Water Vapor Permeation and Morphology of Polysulfone Membranes Prepared by Phase Inversion. *Polímeros* **2020**, *30*, No. e2020027.
(41) Wijaya, O.; Hartmann, P.; Younesi, R.; Markovits, I. I. E.; Rinaldi, A.; Janek, J.; Yazami, R. A Gamma Fluorinated Ether as an Additive for Enhanced Oxygen Activity in Li−O_2 Batteries. *J. Mater. Chem. A* **2015**, *3*, 19061.
(42) Wan, H.; Mao, Y.; Liu, Z.; Bai, Q.; Peng, Z.; Bao, J.; Wu, G.; Liu, Y.; Wang, D.; Xie, J. Influence of Enhanced O_2 Provision on the Discharge Performance of Li−Air Batteries by Incorporating Fluoroether. *ChemSusChem* **2017**, *10*, 1385.
(43) Opitz, M.; Yue, J.; Wallauer, J.; Smarsly, B.; Roling, B. Mechanisms of Charge Storage in Nanoparticulate TiO_2 and $Li_4Ti_5O_{12}$ Anodes New Insights from Scan Rate-Dependent Cyclic Voltammetry. *Electrochim. Acta* **2015**, *168*, 125−132.
(44) Li, K.; Zhang, J.; Lin, D.; Wang, D.-W.; Li, B.; Lv, W.; Sun, S.; He, Y.-B.; Kang, F.; Yang, Q.-H.; Zhou, L.; Zhang, T.-Y. Evolution of the Electrochemical Interface in Sodium Ion Batteries with Ether Electrolytes. *Nat. Commun.* **2019**, *10*, 725.
(45) Khairy, M.; Mahmoud, B. G.; Banks, C. E. Simultaneous Determination of Codeine and its Co-formulated Drugs Acetaminophen and Caffeine by Utilising Cerium Oxide Nanoparticles Modified Screen-Printed Electrodes. *Sens. Actuators, B* **2018**, *259*, 142−154.
(46) Choi, W.; Shin, H.-C.; Kim, J. M.; Choi, J.-Y.; Yoon, W.-S. Modeling and Applications of Electrochemical Impedance Spectroscopy (EIS) for Lithium-Ion Batteries. *J. Electrochem. Sci. Technol.* **2020**, *11*, 1−13.
(47) Cherian, C. T.; Sundaramurthy, J.; Reddy, M. V.; Kumar, P. S.; Mani, K.; Pliszka, D.; Sow, C. H.; Ramakrishna, S.; Chowdari, B. V. R. Morphologically Robust $NiFe_2O_4$ Nanofibers as High Capacity Li-Ion Battery Anode Material. *ACS Appl. Mater. Interfaces* **2013**, *5*, 9957−9963.
(48) Liu, X.; Ma, X.; Wang, J.; Liu, X.; Chi, C.; Liu, S.; Zhao, J.; Li, Y. The Binder-Free $Ca_2Ge_7O_{16}$ Nanosheet/Carbon Nanotube Composite as a High-Capacity Anode for Li-Ion Batteries with Long Cycling Life. *RSC Adv.* **2016**, *6*, 107040.
(49) Khamsanga, S.; Pornprasertsuk, R.; Yonezawa, T.; Mohamad, A. A.; Kheawhom, S. δ-MnO_2 Nanofower/Graphite Cathode for Rechargeable Aqueous Zinc Ion Batteries. *Sci. Rep.* **2019**, *9*, 8441.
(50) Yap, W. T.; Doane, L. M. Determination of Diffusion Coefficients by Chronoamperometry with Unshielded Planar Stationary Electrodes. *Anal. Chem.* **1982**, *54*, 1437−1439.
(51) Zhou, D. B.; Vander Poorten, H. Electrochemical Characterisation of Oxygen Reduction on Teflon-Bonded Gas Diffusion Electrodes. *Electrochim. Acta* **1995**, *40*, 1819−1826.
(52) Nicodemo, L.; Marcone, A.; Monetta, T.; Mensitieri, G.; Bellucci, F. Transport of Water Dissolved Oxygen in Polymers via Electrochemical Technique. *J. Membr. Sci.* **1992**, *70*, 207−215.
(53) Gilbert, R.; Nguyen, H. P.; Jalbert, J.; Charbonneau, S. Transport Properties of a Mixture of Permanent Gases and Light Hydrocarbons Through the Polytetrafluoroethylene Capillary Tubes of a GP-100 Gas Extractor. *J. Membr. Sci.* **2004**, *236*, 153−161.

https://doi.org/10.1021/acs.iecr.1c04244
Ind. Eng. Chem. Res. 2022, 61, 2633−2642